

***K-LM* and *K-MM* radiative Auger effect from Kr and Xe**

A. Mühleisen and M. Budnar

*J. Stefan Institute, P.O. Box 3000, SI-1001 Ljubljana, Slovenia*

J.-Cl. Dousse

*Physics Department, University of Fribourg, CH-1700 Fribourg, Switzerland*

(Received 24 April 1996)

The *K-LM* and *K-MM* radiative Auger (RA) x-ray spectra of Kr and Xe were measured. The transitions were photoinduced by an x-ray tube and measured with a high-resolution transmission curved-crystal spectrometer. For Kr the *K-LM* and *K-MM* RA yields, relative to the  $K\alpha_{1,2}$  and  $K\beta_{1,3}$  lines, were found to be  $0.15\% \pm 0.04\%$  and  $0.77\% \pm 0.2\%$ , respectively. For Xe, only an upper limit of 0.008% relative to the  $K\alpha_{1,2}$  line could be deduced for the *K-LM* RA yield, whereas the total relative intensity of the unresolved *K-M<sub>4,5</sub>M<sub>4,5</sub>* and *K-M<sub>1</sub>N<sub>1</sub>* RA transitions was found to be  $0.06\% \pm 0.02\%$  relative to the  $K\beta_{1,3}$  line. In addition, the Xe *K-M<sub>2,3</sub>N<sub>1</sub>*, *K-M<sub>1</sub>N<sub>4,5</sub>*, and *K-M<sub>1</sub>N<sub>2,3</sub>* RA transitions of Xe were also observed with a total relative intensity of  $0.05\% \pm 0.02\%$ . [S1050-2947(96)08010-9]

PACS number(s): 32.30.Rj, 32.70.Fw, 32.80.Dz, 32.80.Hd

**I. INTRODUCTION**

The radiative Auger (RA) effect is an alternative decay channel of inner shell holes in which one photon and one electron are emitted simultaneously. The electron is either promoted into a higher bound orbital or ejected into the continuum [1]. The transition energy is shared out among the photon and the electron. The RA effect can provide important information on the many-particle interaction in the atom. Experimental data are, however, scarce (especially for *K-LM* RA), while the inconsistencies between the experimental data and the available shake-off (up), configuration interaction (CI), and radiative field calculations are still considerable [2,3]. A complete calculation of *K-MM*, *K-LM*, and *K-LL* RA intensities covering a broad range in the atomic number  $Z$  was done in the shake model only [2]. A detailed calculation of the *K-MM* RA spectrum was also performed but only for Ar [3].

Experimental RA data are in general obtained from fluorescence spectra. In such spectra RA transitions appear as weak and asymmetric profiles superimposed on the low-energy tails of the diagram lines. It has to be noted, however, that the RER (radiative electron rearrangement) and x-ray internal Raman scattering can also contribute to the surplus of intensity characterizing the low-energy tails of the diagram lines. In addition, characteristic lines of trace elements may also be present in the same energy region. A successful observation of RA structures requires therefore a high instrumental resolution of the order of a few eV, and even then the different contributions can be distinguished only under the assumption of a good understanding of the ionization and decay processes.

The present study concerns *K-LM* and *K-MM* RA yields of Kr ( $Z=36$ ) and Xe ( $Z=54$ ). Noble gases were chosen because they are not affected by solid state or molecular structure effects.

**II. EXPERIMENTAL SETUP**

The measurements were performed at the University of Fribourg with a transmission type curved-crystal spectrometer operated in the modified DuMond slit geometry (Fig. 1). A detailed description of a similar spectrometer installed at PSI, Villigen, Switzerland, can be found in [4]. The angular range of the Fribourg instrument is, however, larger ( $\pm 20^\circ$  compared to  $\pm 10^\circ$  at PSI), so that the RA spectra of Kr could be measured. In addition, the distance between the crystal and the detector is also larger (2.89 m compared to 1.5 m at PSI), which results in improved peak-to-background ratios.

The target was a cylindrical cell filled with 99.99% pure noble gas. The gas pressure was close to 3 bars, except for the Kr *K-MM* RA measurements, for which it was 2 bars. The cell was 3 cm in diameter and 3 cm high with a 77.5  $\mu\text{m}$  thick kapton wall. The axis of the cylindrical target was located 2.75 cm behind the slit. Only a vertical slice (with a thickness of  $\sim 0.2$  mm for the 0.15 mm slit and  $\sim 0.15$  mm for the 0.10 mm slit) contributed thus to the production of the measured x rays. The slit was positioned on the focal circle of the spectrometer and served as the effective source of the radiation.

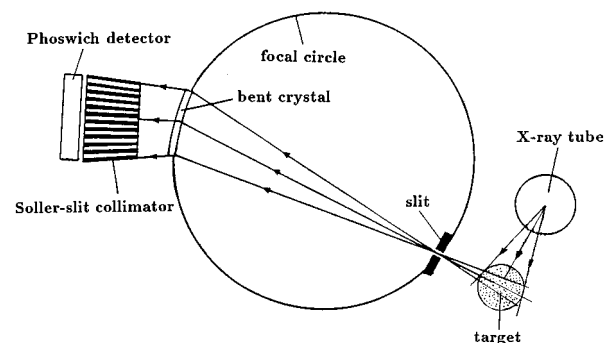


FIG. 1. Schematic view of the experimental setup.

For the photoionization an x-ray tube with a beryllium window was used. The distance between the tube and the center of the cell was 4.5 cm. The angle between the incident radiation from the tube anode and the target-to-crystal direction was  $90^\circ$ . For the photoionization of Xe a Au x-ray tube operated at 80 kV and 30 mA was used. Due to the possible coherent scattering of characteristic Au *L* x-ray radiation from the tube anode in the target chamber, a 0.9 mm thick Al absorber was placed in front of the tube beryllium window for the Kr *K-MM* RA measurements. To exclude these scattered tube x-ray lines from the spectral region of interest, the Kr *K-LM* RA measurements were done with a Cr x-ray tube operated at 85 kV and 30 mA.

For the diffraction of x rays the (110) planes of a 1 mm thick quartz crystal, bent cylindrically to a radius of 313 cm, were used. The reflective area was  $55 \times 48 \text{ mm}^2$ . The reflection angles were measured with an optical laser interferometer with an accuracy of a few marc s.

In front of the detector a Soller slit collimator consisting of 24, 660 mm long, 110 mm high, and 2 mm wide slits was mounted. For the x-ray detection a 5 in.  $\times$  0.25 in. NaI(Tl)  $\times$  2 in. CsI(Tl) Phoswich scintillation detector with a 0.025 mm thick Al window was employed. The signals from the rear CsI crystal were used as anticoincidence gates, so that most of the Compton events in the front crystal could be suppressed. Due to the presence of the *K* absorption edge of iodine in the *K-MM* RA spectrum of Xe, which resulted in an abrupt change of the detector efficiency, this measurement was repeated by replacing the Phoswich detector by a 5 cm in diameter and 1 cm thick high-purity Ge semiconductor detector. The Phoswich and Ge detectors were placed in thick Pb-Cu-Al shielding in order to reduce the background. An additional diminution of the latter was obtained by choosing appropriate energy windows in the analog-to-digital converter (ADC) spectra.

In order to reduce the absorption of x rays, two evacuated tubes were installed between the target and the crystal and between the crystal and the collimator, which was also evacuated. For the Kr *K-MM* RA measurements the target chamber was evacuated, too.

The instrumental response of the spectrometer was determined according to the measurements and procedures presented in [5]. This response, which depends mainly on the slit width, crystal mosaicity, and crystal curvature precision, could be well described in the present experiment by a Gaussian profile of 11.5 arc s full width at half maximum (FWHM).

### III. EXPERIMENTAL METHOD

All spectra were measured in the first order of reflection. For each RA region the energy calibration of the transmission spectrometer was performed by measuring the  $K\alpha_{1,2}$  and  $K\beta_{1,3}$  transitions of the studied element on both sides of reflection. The angular ranges corresponding to the diagram lines and related (*K-LM* or *K-MM*) RA regions were observed in several step by step scans. Each scan consisted of a longer measurement of the RA region and a shorter one of the parent diagram line. With this method of measurement, the systematic errors resulting from uncontrolled intensity changes (due to leakage in the gas chamber or fluctuations in

the x-ray tube intensity) were minimized. In addition, residual fluctuations were accounted for by normalizing off line each RA scan with the intensity of the diagram line measured during the same scan. The RA spectra were then built up by summing off line the different weighted scans.

The total acquisition times per point used to scan the *K-LM* and *K-MM* RA regions of Kr and Xe were 2800, 1500, 2080, and 3900 s, respectively. As mentioned before, the upper energy region of the *K-MM* RA spectrum of Xe was also measured, using a Ge detector for the detection of the diffracted photons. In this case, the total acquisition time per point was 6900 s. Possible instrumental asymmetries were checked by performing shorter measurements on both sides of reflection. No such asymmetry was found, except the background, which was slightly lower on the reflection side used for the measurements.

### IV. DATA ANALYSIS

The high-energy onsets of RA shake-off transitions (electron ejected into the continuum with zero kinetic energy) are equal in energy to the energies of the corresponding Auger transitions. These energies were obtained either directly from [6] or according to [7] as

$$E(KX_j Y_k) = E(K\alpha) + E(L_3 X_j Y_k). \quad (1)$$

The energies were also calculated with the program package GRASP [8]. They were obtained by computing the differences between the energy of the atomic state with an initial *1s* hole and the energies of the atomic states after the RA shake-off transition:

$$E_{\text{edge}} = \max(E[1s] - E[nl, n'l']). \quad (2)$$

Here *nl* and *n'l'* denote holes in the final RA state of a particular RA transition group. max means that the RA transition, having the highest energy, is taken as the onset energy. These energies were used for the identification of the RA transitions.

Because RA structures are composed of several overlapping transitions, the RA onsets are in general smeared out and the observed slope of the onsets does not therefore correspond necessarily to a single transition. For this reason, the high-energy onsets of the RA transitions were determined as follows. First the highest energy for which the intensity starts to rise significantly above the descending tail of the spectrum was looked for. From this maximum energy an energy interval corresponding to half of the width of the parent diagram line at 1/10 of its maximum intensity was then subtracted to obtain the RA energy onset.

In addition, the transition shape was considered to determine whether the observed structure stems from RA or not. The competitive processes that can contribute in the same energy region to the enhancement of the tail intensity (RER, internal Raman scattering, characteristic lines of trace elements) have indeed usually either different energies, different shapes, or both.

For Kr the internal Raman scattering of  $K\beta_{1,3}$  x rays on *3d* electrons could overlap with Kr *K-MM* RA transitions.

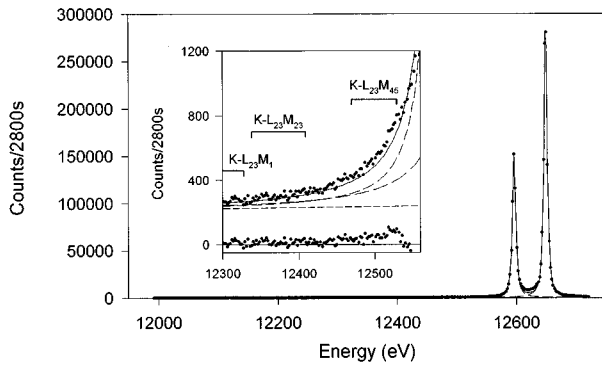


FIG. 2. Kr  $K-LM$  RA spectrum, with enlarged view of the RA region (upper part of the inset). The extracted RA spectrum is shown in the lower part of the inset. The Voigt profiles (each on the whole background) and the background of the fit are presented with dashed lines. The shake-off high-energy onsets, calculated from [6] are marked.

Although the intensity of such Raman scattering lines is expected to be very low [9], check measurements were performed with different pressures in the gas chamber. No change in the shape of the RA spectrum or in its relative intensity was observed, so that the contribution of the Raman scattering to the observed structures was ruled out.

The observed characteristic lines were analyzed with a least-squares-fit program (package MINUIT, CERN library) using Voigt profiles. The Voigt profile results from the convolution of a Lorentzian representing the natural line shape with a Gaussian representing the experimental broadening. In general, the characteristic lines were fitted with a single Voigt profile. The Gaussian width was kept fixed at its known value, whereas the Lorentzian widths, which are not well known for Kr and Xe [10,11], were left free in the fitting procedure. The RA intensities were determined as follows. First the region of the spectrum containing the characteristic lines was fitted. Using the values of the fitting parameters obtained in this first part of the analysis, the rest of the spectrum was fitted, the intervals where RA transitions were observed being, however, excluded. The total RA intensity was finally obtained by computing the difference between the measured spectrum and the fitted one.

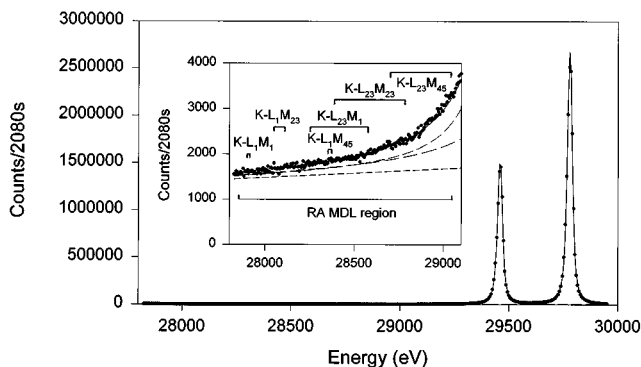


FIG. 3. Xe  $K-LM$  RA spectrum, with enlarged view of the RA region (upper part of the inset). The RA energy region used for the determination of the MDL is also marked in the inset. The dashed lines and the markings have the same meaning as in Fig. 2.

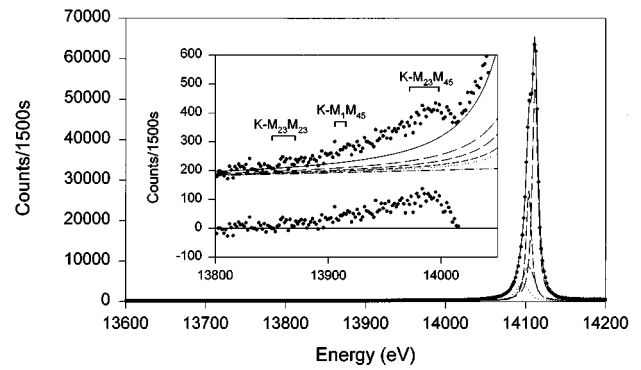


FIG. 4. Kr  $K-MM$  RA spectrum, with enlarged view of the RA region (upper part of the inset). The extracted RA spectrum is shown in the lower part of the inset. The dashed lines and the markings have the same meaning as in Fig. 2.

The above procedure was used for the analysis of the  $K-LM$  RA plus  $K\alpha_{1,2}$  spectrum of Kr. Only the RA contributions from the  $K-L_{2,3}M_{4,5}$  transitions in Kr were clearly seen. The Kr  $K-LM$  RA intensity was obtained by subtracting the fitted diagram lines and linear background from the total spectrum in the RA region. The corresponding spectrum is presented in Fig. 2. In this figure, as well as in Figs. 3, 4, and 5, the intensity of the characteristic lines is normalized to the acquisition time used for the measurement of the RA region.

The  $K\alpha_1$  and  $K\alpha_2$  lines of Xe were fitted in the same way as those of Kr (Fig. 3). For the Xe  $K-LM$  RA yield only an upper limit, equal to the minimum detection limit (MDL) of our experiment, was possible to obtain (see Sec. V).

The fit method used for the  $K\alpha$  lines of Kr failed for the  $K\beta_1$  and  $K\beta_3$  lines due to an asymmetry affecting the low-energy side of the peaks. This asymmetry, present on both sides of reflection ( $n = \pm 1$ ) for the  $K\beta_{1,3}$  lines, was not observed in the case of  $K\alpha_{1,2}$  transitions. Nevertheless, we are inclined to attribute this intriguing effect to the bent crystal. The  $K\beta_1$  and  $K\beta_3$  lines of Kr were fitted for this reason with two Voigt functions each. All parameters were left free in the fitting procedure, except the  $K\beta_3/K\beta_1$  ratio, which was kept at 0.5111 [2]. Furthermore, as there are no reliable theoretic

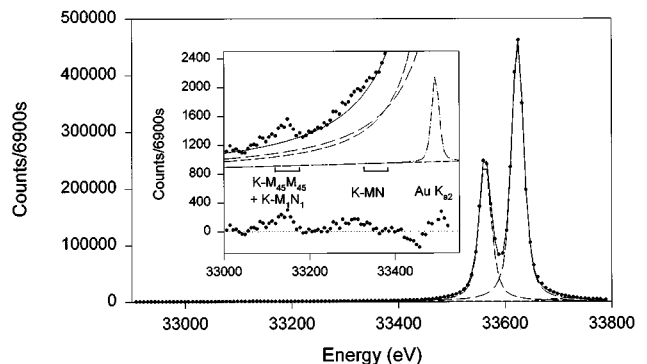


FIG. 5. Xe  $K-MM$  RA spectrum, with enlarged view of the RA region (upper part of the inset). The fit of the scattered Au  $K\alpha_2$  line is also represented. The difference between the fit and the spectrum is shown in the lower part of the inset. The dashed lines and the markings have the same meaning as in Fig. 2.

TABLE I. Experimental and theoretical RA shake-off high-energy onsets in eV.

RA transition	RA start point	Expt. edge	Larkins	GRASP
Kr $K-L_{2,3}M_{4,5}$	12537 ± 3	12528	12529.1	12525.6
Kr $K-M_{2,3}M_{4,5}$	14010 ± 3	13998	13998.4	13998.5
Xe $K-M_{4,5}M_{4,5}$	} 33184 ± 7	} 33151	33175.0	33165.6
Xe $K-M_1N_1$			33180.5	33168.1
Xe $K-M_{2,3}N_1$	} 33356 ± 7 <sup>a</sup>	} 33323	33248.9	33233.5
Xe $K-M_1N_{4,5}$			33330.0	33325.3
Xe $K-M_1N_{2,3}$			33387.0	33374.7

<sup>a</sup>Edge smeared out, starts with a very weak slope.

cal or experimental data on  $K\beta_1$  and  $K\beta_3$  Kr linewidths and because the measured lines were asymmetrical, we did not fix the Gaussian widths. The spectrum corresponding to the low-energy tails of the  $K\beta_{1,3}$  transitions (RA regions excluded) was then fitted, the Lorentzian and Gaussian widths being kept fixed at the values obtained in the preceding fit of the  $K\beta_{1,3}$  lines. The low-energy tail spectrum and its fitting function are depicted in Fig. 4. The RA intensity was obtained by computing the difference between them.

In the  $K-MM$  RA spectrum of Xe, the RA structure lies close in energy to the  $K\beta_3$  line and is thus very sensitive to the method used to fit the data. For this reason the  $K\beta_1$  and  $K\beta_3$  lines of Xe were fitted with a single Voigt profile each, the Lorentzian and Gaussian widths being left free in the fitting procedure. An additional reason for not keeping fixed the Gaussian width lay in the fact that the instrumental response of the spectrometer equipped with the Ge detector was not precisely known. Due to the smaller diameter of the latter (5 cm compared to the 5 in. for the Phoswich detector), only the central part of the crystal contributes to the reflection of the x rays, which results in general in a reduction in the width of the instrumental response. Actually the Gaussian widths obtained from the fits of the  $K\beta_1$  and  $K\beta_3$  were found to be for both detectors in good agreement with the values determined previously [5]. Furthermore, the Lorentzian widths were also found to be consistent within the experimental uncertainties with the values quoted in Ref. [12]. A slight asymmetry on the high-energy side of the diagram lines (relative intensity of  $\sim 2 \times 10^{-3}$ ) was observed. This asymmetry, which was attributed to unresolved  $M$  satellites, was accounted for by the use in the fit of an additional Voigt profile. The  $K\beta_5$  line with  $\sim 1.0\%$  intensity relative to  $K\beta_{1,3}$  was also included in the fit. In the energy region of the Xe  $K-MM$  RA (32.0–33.2 keV) only the iodine absorption edge was observed when measured with the Phoswich detector. The measurements repeated with the Ge detector re-

TABLE II. Relative  $I(K-LM \text{ RA})/I(K\alpha_{1,2})$  yields (in %) for Kr and Xe.

Element	Z	Experiment	Theory	One RA transition
Kr	36	0.15 ± 0.06	0.18	0.11 ± 0.05 <sup>a</sup>
Xe	54	≤ 0.008	0.075	≤ 0.0036

<sup>a</sup>In the energy region where only  $K-L_{2,3}M_{4,5}$  is energetically possible.

vealed weak structures above 32.9 keV, manifested as three separate bumps on the tail of the  $K\beta_{1,3}$  line. These structures could be extracted. The highest bump was identified as a second order reflection of the Au  $K\alpha_2$  line originating from the x-ray tube anode and coherently scattered in the target. This bump was included in the fit of the characteristic lines and fitted as a peak. The region of the other two bumps was excluded from the fit of the  $K\beta_{1,3}$  line. Their intensities were again obtained by computing the difference between the total spectrum and the fitted one (Fig. 5).

## V. RESULTS

The energies of the RA shake-off high-energy onsets were extracted from the spectra and compared with theoretical predictions (Table I). The theoretical predictions marked ‘‘Larkins’’ were obtained according to Eq. (1) and the GRASP predictions according to Eq. (2).

All deduced RA intensity ratios relatively to the intensities of the characteristic lines ( $K\alpha_{1,2}$  and  $K\beta_{1,3}$ , respectively) were corrected for the self-absorption in the target, the x-ray intensity attenuation between the target and the detector, and for the iodine absorption edge of the Phoswich detector. The results are presented in Tables II–IV together with the available theoretical estimates [2].

The measured Kr  $K-LM$  RA x-ray distribution (Fig. 2) was ascribed mainly to the  $K-L_{2,3}M_{4,5}$  RA transitions because no onset of other RA transitions was observed. A minimum intensity of the  $K-L_{2,3}M_{4,5}$  RA transitions was also determined from the net intensity observed in the region where other RA transitions are not allowed (Table II).

As mentioned before, no obvious RA structure was observed in the  $K\alpha$  spectrum of Xe (Fig. 3). Therefore, for this

TABLE III. Relative  $I(K-MM \text{ A})/I(K\beta_{1,3})$  yields (in %) for Kr and Xe.

Element	Z	Experiment	Expt. one RA transition	Theory [2]
Kr	36	0.77		2.11
Xe	54	0.062 ± 0.02 <sup>a</sup>	0.062 ± 0.02 <sup>a</sup>	0.55
Xe <sup>b</sup>	54	≤ 0.02 <sup>c</sup>	≤ 0.01 <sup>d</sup>	

<sup>a</sup>The  $K-M_{4,5}M_{4,5}$  and the  $K-M_1N_1$  transitions together.

<sup>b</sup>Measurement with Phoswich detector.

<sup>c</sup>Upper limit for RA without the  $K-M_{4,5}M_{4,5}$ .

<sup>d</sup>Upper limit for one RA group except the  $K-M_{4,5}M_{4,5}$ .

TABLE IV. Relative  $I(\text{Xe } K\text{-}MN \text{ RA})/I(\text{Xe } K\beta_{1,3})$  yields in %.

RA transition	Intensity
$K\text{-}M_{4,5}M_{4,5}+K\text{-}M_1N_1$	$0.062 \pm 0.020$
$K\text{-}M_{2,3}N_1+K\text{-}M_1N_{4,5}+K\text{-}M_1N_{2,3}$	$0.052 \pm 0.020$
$K\text{-}MN$ all, theory [2]	0.52

element, only an upper limit could be deduced for the relative  $K\text{-}LM$  RA yields. For the determination of this upper limit which corresponds to the minimum detection level of our experiment, the background fluctuations in the RA region were considered relative to the intensity of the  $K\alpha_{1,2}$  diagram line. A value equal to three times the square root of the background was used as an estimate of the background fluctuations.

In the Kr  $K\text{-}MM$  RA spectrum the  $K\text{-}M_{4,5}M_{4,5}$  RA transitions were not noticeable because they are too close to the  $K\beta_{1,3}$  line and lie high on the low-energy tail of the latter. In addition, the  $K\beta_{1,3}$  line shape is slightly asymmetric, as mentioned before. Therefore all measured Kr  $K\text{-}MM$  RA relative intensities stem from lower lying transitions, mostly  $K\text{-}M_{2,3}M_{4,5}$  RA (Fig. 4).

The Xe  $K\text{-}MM$  RA spectrum was first observed with the standard spectrometer setup (Phoswich detector). No RA structure was observed below 33 keV. Above this energy the shape of the spectrum was somewhat dubious due to the presence of the iodine  $K$  absorption edge at 33.170 keV. The Phoswich detector was thus replaced by a  $\sim 20 \text{ cm}^3$  Ge semiconductor detector and the energy region above 33 keV was scanned a second time. The spectrum corresponding to that second scan is depicted in Fig. 5. The  $K\text{-}M_{4,5}M_{4,5}$  RA transitions with the energy onset at  $E=33175 \text{ eV}$  overlap with the  $K\text{-}M_1N_1$  RA transitions. The group of  $K\text{-}M_{2,3}N_1$ ,  $K\text{-}M_1N_{4,5}$ , and  $K\text{-}M_1N_{2,3}$  RA transitions was also seen at slightly higher energies than the  $K\text{-}M_1N_1$  RA group (Fig. 5 and Table IV). At  $\sim 33495 \text{ eV}$  an additional sharp peak, identified as the second order Bragg reflection of the Au  $K\alpha_2$  line, was observed. Its energy, as found in the literature,

TABLE V. Relative  $I(K\text{-}LM \text{ RA})/I(K\alpha_{1,2})$  yields in % (available experimental results and theoretical estimates). Experimental data are from Ref. [16], except where noted.

Element	Z	Experiment	Theory [2]
Ar	18		0.76
Ca	20	0.11 <sup>a</sup>	0.68
Ti	22	0.12 <sup>a</sup>	0.60
V	23	0.17	0.56
Cr	24	0.27	0.52
Mn	25	0.18	0.49
Fe	26	0.17	0.46
Cu	29	0.11 <sup>b</sup>	0.36
As	33	0.68	0.26
Kr	36	$0.15 \pm 0.04$ <sup>c</sup>	0.18
Xe	54	$\leq 0.008$ <sup>c</sup>	0.075

<sup>a</sup>[13] (uncertainty  $\pm 40\%$ ).<sup>b</sup>[17] estimated 0.03 for  $K\text{-}L_3M_{4,5}$  transition.<sup>c</sup>This work.TABLE VI. Relative  $I(K\text{-}MM \text{ RA})/I(K\beta_{1,3})$  yields in % (available experimental results and theoretical estimates).

Element	Z	Experiment	Theory [2]	Theory <sup>a</sup> [9]
P	15	3.80		
S	16	4.00		
Cl	17	6.90		
Ar	18	5		7.73
K	19	4.75		
Ca	20	3.90 3.14		
Sc	21	3.20		
Ti	22	2.60 2.40 2.44		
V	23	2.30 3.70		
Cr	24	2.00 3.15 2.91		
Mn	25	2.40 2.45		
Fe	26	1.60 3.45 0.40	4.07	
Co	27	1.40	3.95	1.94
Ni	28	1.20	3.75	1.74
Cu	29	1.10 2.05	3.59	1.60
Zn	30	1.40	3.43	1.45
As	33	1.90		
Kr	36	$0.77 \pm 0.20$ <sup>b</sup>	2.11	
Mo	42	1.14	1.34	
Ru	44	1.36	1.16	
Pd	46	0.99	1.00	
Cd	48	0.46	0.86	
Sn	50	0.36	0.75	
Xe	54	$\leq 0.06 \pm 0.02$ <sup>c</sup>	0.55	

<sup>a</sup>Only  $3s$  and  $3p$  electrons.<sup>b</sup>This work, the  $K\text{-}M_{4,5}M_{4,5}$  were not observed.<sup>c</sup>This work, the  $K\text{-}M_1N_1$  are included.

is  $66\,991.16 \text{ eV}$  [11]. This energy was diminished by  $0.6 \text{ eV}$  in accordance with the estimated additional corrections for the data from [11], presented in [12]. The Au  $K\alpha_2$  line intensity, stemming from the coherent scattering in the target of the characteristic x-ray emission from the tube anode, was  $0.12\%$  relative to the Xe  $K\beta_{1,3}$  line intensity. As the energy of this Au line coincides in second order with that of the Xe  $K\text{-}M_{2,3}N_{4,5}$  RA transitions, the latter could not be observed.

The relative  $K\text{-}M_{4,5}M_{4,5}$  RA yield of Xe is given in Table III. For other  $K\text{-}MM$  RA transitions of Xe only upper limits are listed. The latter were determined with the method presented above. The first upper limit was deduced from the background fluctuations in the whole  $K\text{-}MM$  RA region with the exclusion of the  $K\text{-}M_{4,5}M_{4,5}$  domain ( $32.2\text{--}33.1 \text{ keV}$ ) whereas the second one corresponds to the average value obtained for a  $200 \text{ eV}$  wide energy interval lying in the region of interest. The value of  $200 \text{ eV}$  was chosen because it corresponds approximately to the energy extension of the different  $K\text{-}M_iM_j$  RA groups.

## VI. DISCUSSION

### A. General

The experimental data of  $K\text{-}LM$  and  $K\text{-}MM$  RA known up to now [13–15] and the theoretical estimates [2] are presented in Tables V and VI. In a previous study devoted to the  $K\text{-}MM$  RA spectrum of Ar [3], RA transitions to bound

states were observed. Figures 2–5 show that this is not the case in our experiment. Such transitions are indeed less likely at higher  $Z$ , as can be seen from the electron shake-off/shake-up ratios which are decreasing with growing  $Z$  [18]. Although the resolution of the experimental setup was sufficient, the statistics needed to observe the transitions to bound states was not achieved. The RA transitions to continuum states have the highest intensity at the RA high-energy onset and then the intensity goes down continuously until the x ray has a vanishing energy. This makes the identification and the determination of the partial intensities of weaker RA transitions, positioned on the tail of stronger ones, more difficult. The only available RA calculations performed for Kr and Xe were done within the shake model [2,19]. In these calculations, only total RA intensities are given. Some discrepancy between the experiment and theory is caused by the vanishing of the low-energy tails of the measured RA transitions in the background. Although their intensity per energy interval is extremely low, their extension down to zero x-ray energy is so broad that they can appreciably contribute to the total RA intensity.

### B. K-LM RA transitions

High-resolution  $K$ -LM RA measurements with quantitative results were done only for Ca and Ti [13]. Other quantitative measurements were performed with semiconductor detectors and were devoted to the determination of the  $K\beta/K\alpha$  intensity ratios, so that it was not even expected that the  $K$ -LM RA yields would be accurate [16]. In our Kr  $K$ -LM RA results only the onset of the  $K$ - $L_{2,3}M_{4,5}$  RA transition was observed and the whole Kr  $K$ -LM RA intensity determined (Table II). Our result agrees, within the experimental error, with the shake model prediction. In the Xe spectra no  $K$ -LM RA transition was observed. The deduced upper limit is much smaller than the shake model prediction (Table II). Since there is no other experiment except ours giving  $K$ -LM yields for elements as heavy as Xe, it is difficult to conclude that the shake model calculations fail for high  $Z$ . It has to be noted, however, that, even if the shake contribution prevails among other RA mechanisms for low- $Z$  elements, this might not be true at higher  $Z$ .

### C. K-MM RA transitions

The  $K$ -MM RA data base is the biggest one, because the  $K$ -MM transitions are the most intense RA transitions. Their intensity is high enough to appreciably affect the  $K\beta/K\alpha$  intensity ratios or the results of elemental analysis (PIXE, XRF, etc.) of low- and medium- $Z$  elements. In the present measurements of Kr  $K$ -MM RA only the  $K$ - $M_{2,3}M_{4,5}$  RA onset was observed. The total  $K$ -MM RA yield extracted from our experiment is much smaller than the theoretical prediction (Table III). However, as the  $K$ - $M_{4,5}M_{4,5}$  RA transitions, that are hidden in our measurement by the diagram line, usually contribute half or even more to the whole RA intensity, our result does not necessarily contradict other measurements on elements with similar  $Z$  [15]. In the  $K$ -MM spectrum of Xe, only the  $K$ - $M_{4,5}M_{4,5}$  RA transitions were clearly identified. Since the latter could not be resolved from the overlapping  $K$ - $M_1N_1$  RA transitions, our result of 0.062% relative to the  $K\beta_{1,3}$  intensity for the  $K$ - $M_{4,5}M_{4,5}$  RA

transitions is, however, probably somewhat overestimated. The upper limit of other Xe  $K$ -MM RA transition probabilities was estimated to be 0.01% for one group and 0.02% for all groups together. The disagreement with the shake model predictions is even greater than the one found for the  $K$ -LM transitions, especially if we consider that the intensities of the  $K$ - $M_{4,5}M_{4,5}$  RA transitions are not taken into account by the shake model [2,19] (Table III).

### D. K-MN RA transitions

Besides the  $K$ - $M_1N_1$  RA transitions that are overlapping with the  $K$ - $M_{4,5}M_{4,5}$  RA ones, the groups of  $K$ - $M_{2,3}N_1$ ,  $K$ - $M_1N_{4,5}$ , and  $K$ - $M_1N_{2,3}$  RA transitions with a total relative intensity of 0.052% were also observed. The  $K$ - $M_{2,3}N_{2,3}$  RA transitions whose energies fall in the region between the two above mentioned RA groups were not observed. This is due not only to their low intensity but also to the complex deconvolution of the spectra. In fact, the RA regions are so close together or even overlapping that a correct estimation of the intensity of the weak  $K$ - $M_{2,3}N_{2,3}$  RA group is practically impossible. The Xe  $K$ - $M_{4,5}N_i$  RA transitions, that probably contribute most to the  $K$ -MN RA intensity, were not observed, as they lie above the Xe  $K\beta_1$  line. These RA transitions (as well as  $K$ - $M_{4,5}M_{4,5}$  RA transitions) actually correspond to the “forbidden”  $K\beta_5$  line [20]. Theoretical [2] predictions for Xe  $K$ -MN RA intensity which are 0.52% relative to the  $K\beta_{1,3}$  line are again much greater than the experimental values (Table IV). Here, some of the discrepancy could also arise from the difficulties encountered in the fitting procedure.

## VII. CONCLUSIONS

The  $K$ -LM and  $K$ -MM RA yields of Kr and Xe were determined and compared to other available data and theory. Some  $K$ -MN RA transitions in Xe were also observed. The experimental resolution enabled us to identify some particular groups of RA transitions. However, only total RA yields were deduced due to the partial overlap of the different RA groups.

The measured yields are smaller (for Xe even drastically) than the theoretical predictions, as is the case in most other RA measurements. For a better analysis of the transition probabilities of individual RA transitions, experimental data with an improved statistics are necessary. We would like to emphasize here that there is a lack of quantitative experimental data, especially for  $K$ -LM RA transitions. In addition, the observed differences between experiment and theory call for new RA dedicated theoretical calculations.

## ACKNOWLEDGMENTS

One of the authors (A.M.) wishes to thank his colleagues from the University of Fribourg for their help and acknowledges the financial support of the Ministry of Science and Technology of the Republic of Slovenia. This work was also partly supported by the National Swiss Science Foundation.

- [1] T. Åberg, in *Atomic Inner Shell Processes*, edited by B. Crasemann (Academic Press, New York, 1975), p. 353.
- [2] J. H. Scofield, *Phys. Rev. A* **9**, 1041 (1974).
- [3] V. O. Kostroun and G. B. Baptista, *Phys. Rev. A* **14**, 363 (1976).
- [4] B. Perny, J.-Cl. Dousse, M. Gasser, J. Kern, R. Lanners, Ch. Rhême, and W. Schwitz, *Nucl. Instrum. Methods A* **267**, 120 (1988).
- [5] J. Hozzowska, J.-Cl. Dousse, and Ch. Rhême, *Phys. Rev. A* **50**, 123 (1994).
- [6] F. P. Larkins, *At. Data. Nucl. Data Tables* **20**, 311 (1977).
- [7] A. Servomaa and O. Keski-Rahkonen, *J. Phys. C* **8**, 4124 (1975).
- [8] K. G. Dyllal, I. P. Grant, C. T. Johnson, F. A. Parpia, and E. P. Plummer, *Comput. Phys. Commun.* **55**, 425 (1989).
- [9] O. Keski-Rahkonen, and J. Ahopelto, *J. Phys. C* **13**, 471 (1980).
- [10] S. I. Salem and P. L. Lee, *At. Data. Nucl. Data Tables* **18**, 233 (1976).
- [11] E. G. Kessler, Jr., R. D. Deslattes, D. Girard, W. Schwitz, L. Jacobs, and O. Renner, *Phys. Rev. A* **26**, 2696 (1982).
- [12] T. Mooney, E. Lindroth, P. Indelicato, E. G. Kessler, Jr., and R. D. Deslattes, *Phys. Rev. A* **45**, 1531 (1992).
- [13] A. Mühleisen, M. Budnar, M. Hribar, Ž. Šmit, and M. Ravnikar (unpublished).
- [14] M. Budnar, A. Mühleisen, M. Hribar, H. Janžekovič, M. Ravnikar, Ž. Šmit, and M. Žitnik, *Nucl. Instrum. Methods B* **63**, 377 (1992).
- [15] Ch. Herren and J.-Cl. Dousse, *Phys. Rev. A* **53**, 717 (1996).
- [16] J. L. Campbell, A. Perujo, W. J. Teesdale, and B. M. Millman, *Phys. Rev. A* **33**, 2410 (1986).
- [17] N. Maskil and M. Deutsch, *Phys. Rev. A* **38**, 3467 (1988).
- [18] T. A. Carlson and C. W. Nestor, Jr., *Phys. Rev. A* **8**, 2887 (1973).
- [19] T. Åberg, *Phys. Rev. A* **4**, 1735 (1971).
- [20] F. Bloch, *Phys. Rev.* **48**, 187 (1935).